Published OnlineFirst January 28, 2016; DOI: 10.1158/1535-7163.MCT-15-0165

Models and Technologies

Molecular Cancer Therapeutics

Modeling Therapy Response and Spatial Tissue Distribution of Erlotinib in Pancreatic Cancer

Barbara M. Grüner[1], Isabel Winkelmann[2], Annette Feuchtinger[2], Na Sun[2], Benjamin Balluff[3], Nicole Teichmann[1], Alexander Herner[1], Evdokia Kalideris[1], Katja Steiger[4], Rickmer Braren[5], Michaela Aichler[2], Irene Esposito[6], Roland M. Schmid[1,7], Axel Walch[2], and Jens T. Siveke[1,7,8]

Abstract

Pancreatic ductal adenocarcinoma (PDAC) is likely the most aggressive and therapy-resistant of all cancers. The aim of this study was to investigate the emerging technology of matrix-assisted laser desorption/ionization imaging mass spectrometry (MALDI IMS) as a powerful tool to study drug delivery and spatial tissue distribution in PDAC. We utilized an established genetically engineered mouse model of spontaneous PDAC to examine the distribution of the small-molecule inhibitor erlotinib in healthy pancreas and PDAC. MALDI IMS was utilized on sections of single-dose or long-term–treated mice to measure drug tissue distribution. Histologic and statistical analyses were performed to correlate morphology, drug distribution, and survival. We found that erlotinib levels were significantly lower in PDAC compared with healthy tissue ($P = 0.0078$). Survival of long-term–treated mice did not correlate with overall levels of erlotinib or with overall histologic tumor grade but did correlate both with the percentage of atypical glands in the cancer ($P = 0.021$, $r_s = 0.59$) and the level of erlotinib in those atypical glands ($P = 0.019$, $r_s = 0.60$). The results of this pilot study present MALDI IMS as a reliable technology to study drug delivery and spatial distribution of compounds in a preclinical setting and support drug imaging–based translational approaches. *Mol Cancer Ther; 15(5); 1145–52.* ©*2016 AACR.*

Introduction

Pancreatic ductal adenocarcinoma (PDAC) is likely the most aggressive and therapy-resistant of all cancers (1). PDAC is characterized by a large degree of inter- and intratumoral genetic heterogeneity and a strong desmoplastic reaction, factors that likely impede many therapeutic approaches. Modeling these hallmark characteristics of PDAC *in vivo* using xenograft models has been largely disappointing, while genetically engineered mouse models (GEMM) based on pancreas-specific activation of oncogenic mutant Kras faithfully recapitulate the morphologic and molecular characteristics of human PDAC enabling sophisticated preclinical approaches (reviewed in ref. 2).

Recently, Olive and colleagues found transplanted xenografts to be highly responsive to gemcitabine treatment but not tumors in GEMM due to lower perfusion and high desmoplasia in the latter. These results support the view that GEMM recapitulate the clinically acknowledged stromal barrier potentially better than classical xenotransplant models (3).

Drug tissue distribution and metabolism are key factors for tumor responses to therapy. Despite their extensive use, autoradiography and tissue homogenate LC-MS analysis have limitations in providing a comprehensive assessment of tissue distributions. Matrix-assisted laser desorption/ionization (MALDI) imaging mass spectrometry (IMS) allows the simultaneous label-free detection of multiple molecules while maintaining spatial distribution in tissues, thus allowing various translational approaches (overview in ref. 4). We thus aimed to establish a MALDI IMS–based detection method for preclinical characterization of intratumoral drug delivery in PDAC.

EGFR is a long-known target in many tumors, including PDAC supported by a plethora of clinical and preclinical evidence (5). Erlotinib, a small-molecule tyrosine kinase domain inhibitor directed against EGFR, is to date the only approved targeted therapy for PDAC. However, its clinical benefit in combination with standard chemotherapy gemcitabine is very modest, arguing that additional factors codetermine therapy response. So far, no biomarker for a clinical response except a drug-induced skin rash has been identified. Besides multiple molecular resistance

[1]2. Medizinische Klinik, Technische Universität München, Munich, Germany. [2]Research Unit Analytical Pathology, Helmholtz Center Munich - German Research Center for Environmental Health, Neuherberg, Germany. [3]Center for Proteomics and Metabolomics, Leiden University Medical Center, Leiden, the Netherlands. [4]Institute of Pathology, Technische Universität München, Munich, Germany. [5]Institute of Radiology, Technische Universität München, Munich, Germany. [6]Institute of Pathology, Heinrich-Heine-University, Düsseldorf, Germany. [7]German Cancer Consortium (DKTK) and German Cancer Research Center (DKFZ), Heidelberg, Germany. [8]Division of Solid Tumor Translational Oncology, German Cancer Consortium (DKTK) Partner Site Essen, West German Cancer Center, University Hospital Essen, Essen, Germany.

Note: Supplementary data for this article are available at Molecular Cancer Therapeutics Online (http://mct.aacrjournals.org/).

Current address for B.M. Grüner: Department of Genetics, Stanford University School of Medicine, Stanford, California.

Corresponding Authors: Jens T. Siveke, Division of Solid Tumor Translational Oncology, West German Cancer Center, University Hospital Essen, Hufelandstr. 55, 45147 Essen, Germany. Phone: 49 201 723 3704; Fax: 49 201 723 6725; E-mail: j.siveke@dkfz.de; or Axel Walch, Research Unit Analytical Pathology, Helmholtz Center Munich, German Research Center for Environmental Health, Ingolstädter Landstr. 1, 85764 Neuherberg, Germany. Phone: 49-89-3187-2739; Fax: 49-89-3187-3360; E-mail: axel.walch@helmholtz-muenchen.de

doi: 10.1158/1535-7163.MCT-15-0165

Published OnlineFirst January 28, 2016; DOI: 10.1158/1535-7163.MCT-15-0165

mechanisms (6,7), inefficient drug delivery due to abundant desmoplasia and tumor-independent factors such as interindividual variations in metabolism and modulation of immune responses may account for poor treatment response (8,9). We thus aimed to utilize MALDI IMS to establish and characterize the delivery and distribution of erlotinib in healthy and tumorous pancreatic tissue using a GEMM-based approach.

Materials and Methods

Mouse strains

Kras$^{wt/LSL\text{-}G12D}$, *Ptf1a*$^{wt/Cre}$, and *Trp53*$^{fl/fl}$ strains have been described previously (10–12). Mice were interbred to obtain *Ptf1a*$^{wt/Cre}$;*Kras*$^{wt/G12D}$;*Trp53*$^{fl/fl}$ mice (named *Kras*^{G12D};*p53*^{KO}) and were backcrossed to C57BL/6J background for at least four generations. C57BL/6J mice served as wild-type (WT) controls. All animal experiments were in accordance with German Federal Animal Protection Laws and approved by the Institutional Animal Care and Use Committee at the Technical University of Munich.

Drug treatment of mice

Erlotinib (Roche) was dissolved in 0.5% methylcellulose in water and was administered to mice by oral gavage in either a single dose for indicated time points or daily ± gemcitabine (Cellpharma) as indicated as soon as a tumor was detectable with MRI. For combination treatment, four doses of gemcitabine were administered i.p. each separated by 3 days in the concentration of 100 mg/kg.

MRI measurement of mice

To track tumor onset and end point volume, noninvasive magnetic resonance imaging (MRI) was performed with a clinical 1.5 T MRI scanner as previously described (5). MRI experiments were initiated at an age of 25 to 40 days and were performed weekly. Before imaging, mice were anesthetized by continuous gaseous infusion of 2% isoflurane (Abbott) for at least 10 minutes using a veterinary anesthesia System (Vetland Medical). During imaging, the dose was kept at 2% isoflurane, animal temperature was maintained and continuously monitored, and eyes were protected with an eye ointment. Tumor growth kinetic changes were followed with T2 weighted imaging protocol using microscopy surface coil inside a Philips 1.5 T or 3.0 T clinical scanner. An axial multislice T2-weighted (T2w) TSE sequence (resolution 0.3 × 0.3 × 0.7 mm^3, minimum 30 slices, TE = 90 ms, TR > 3 s) was applied for tumor detection. Solid tumor volumes were calculated using in-house optimized ImageJ-based software that differentiates between solid and cystic parts of the tumor.

MALDI-TOF IMS measurement of erlotinib on pancreatic sections

Pancreata were resected and snap frozen in liquid nitrogen without fixation. Cryosections (10 μm) were cut and transferred to Indium-Tin-Oxide–coated glass slides pretreated with polylysine (0.1 %) 1:1 in water with 0.1% NP-40. Sections were dried for 30 minutes at room temperature, and α-cyano-4-hydroxycinnamic acid (CHCA) matrix (7 g/L CHCA in 70% methanol) was applied to the glass slide with the ImagePrep station (Bruker Daltonics). Mass spectra were measured using the MALDI TOF/TOF Analyzer Ultraflex III (Bruker Daltonics) with a spatial resolution of 70 μm in reflector mode. Ions were detected in a mass range of *m*/*z* 200 to 500 with a sampling rate of 0.1 GS/s. Calibration for each measurement was performed using the first isotope of the matrix dimer (CHCA: $2MH^+ + 1 = 380.09$) as calibration point. MALDI-TOF IMS data were obtained and analyzed using the FlexControl 3.0 and FlexImaging 3.0 software (Bruker Daltonics).

Coregistration of morphology and spectra for MALDI measured sections

After MALDI measurements, slides were washed in 70% ethanol to remove the matrix and counterstained with hematoxylin/eosin (H&E). High-resolution images of stained sections were taken using the Mirax Scan system (Carl Zeiss) and coregistered with the MALDI IMS data to correlate mass spectra with the histologic features of the same section.

Statistical analysis of MALDI IMS data

With the FlexImaging software, regions of interest (ROI) were defined, and 80 to 500 randomly chosen single spectra (depending on sample number and ROI size) per mouse per ROI group were exported to ClinProTools 2.2 software for further analysis. Extracted mass spectra were recalibrated on common "background" peaks (spectral alignment), normalized to their total ion count, and the relative signal intensities for selected ions per ROI were calculated.

Average peak intensities for erlotinib were exported from ClinProTools and compared using the Wilcoxon test for non-normally distributed paired data using the GraphPad Prism5 statistical software. For correlation analyses, Spearman correlation coefficients for nonparametric data and corresponding *P* values for linear regression were calculated. *P* values ≤ 0.05 were considered significant.

To correlate erlotinib distribution and morphology, Definiens Developer XD2 (Definiens AG) was used. A rule set was developed in order to detect and quantify semantic classes. In a first step, the algorithm segment pictures iteratively, recognizing groups of pixels as objects. The objects are classified further based on staining intensity, morphology, neighborhood, and special color features to distinguish the morphologic classes "glandular" and "desmoplastic," and their percentage of total area was calculated. With the same software, the presence of erlotinib on mass-visualization pictures, provided by the Bruker FlexImaging Software, was classified, and overlay with the above-defined morphologic classes was calculated.

MALDI FT-ICR IMS measurement of erlotinib and related metabolites on pancreatic sections

Fourier transform ion cyclotron resonance (FT-ICR) measurements were performed using the Solarix 7T (Bruker Daltonics). Mass spectra were acquired in positive mode using 300 laser shots at a frequency of 1 kHz. MSI data were recorded with a 50-μm spatial resolution. The digital resolution of the MALDI FT-ICR was 150,000 at *m*/*z* 400. Consequently, MALDI FT-ICR enables simultaneous imaging of the low abundant metabolites of erlotinib, including M13, M14, M16, and M6 (13).

Results

Determination of time point for highest drug concentration

To analyze the distribution and pharmacokinetics of *in vivo* administered erlotinib in the pancreas, 25 mg/kg erlotinib diluted in methylcellulose were administered orally to WT mice ($n = 3$ mice for each time point plus one vehicle only treated control for

Published OnlineFirst January 28, 2016; DOI: 10.1158/1535-7163.MCT-15-0165

each time point to determine baseline levels). The average peak intensity for erlotinib [$(M+H^+) = 394.18$ Da] could be detected in pancreata of mice treated with the drug 0.5, 1, 4, and 12 hours after drug administration. No peak corresponding to the mass of erlotinib could be detected in pancreata of control (vehicle-treated) mice, ensuring specific drug detection. Twenty-four hours after drug administration, the relative levels of erlotinib returned to untreated control levels, showing full metabolic elimination of the drug. One hour after drug application, average peak intensities were highest (Fig. 1A), and this time point was chosen for further analysis in PDAC-bearing mice.

Erlotinib levels are higher in healthy pancreas than in PDAC

To determine the distribution and relative peak intensities of erlotinib in normal, preneoplastic. and tumor tissue, 8 *Ptf1a*$^{wt/Cre}$;*Kras*$^{wt/LSL\text{-}G12D}$;*p53*$^{fl/fl}$ (named *Kras*^{G12D};*p53*^{KO} hereafter) mice at approximately 6 weeks of age were treated with a single dose of erlotinib. At this age, mice display well-differentiated PDAC with abundant stroma (14,15) next to still healthy acinar tissue. The two-dimensional tissue distribution image of relative erlotinib peak intensities for each of the analyzed tumor sections depicted differences in drug distribution between healthy pancreatic tissue and PDAC with increased amounts of erlotinib in healthy acinar tissue but only low average peak intensities in tumor areas (example in Fig. 1B). Statistical analysis revealed significantly less average erlotinib peak intensities ($P = 0.0078$) in tumorigenic tissue than in acinar tissue within each mouse (Fig. 1C), supporting impaired delivery of erlotinib into the tumor tissue. High levels of drug peak intensities at the outer borders of the lymph nodes and nearly no signal in the middle of the nodes indicate that the drug uptake follows the lymph flow in the lymph nodes from subcapsular sinus to medulla (Fig. 1B). "On tissue" spotting of erlotinib confirmed the differences in peak intensities were not due to ion suppression (Supplementary Fig. S1A and Supplementary Materials and Methods). "On tissue" MS/MS spectrum of erlotinib (m/z 394) comparison to reference erlotinib confirmed the specific identification of erlotinib (Supplementary Fig. S1B and Supplementary Materials and Methods). In addition, we performed high mass resolution MALDI FT-ICR analysis on selected sections to visualize the differences in intensities of the parent drug erlotinib and its main metabolite M13/14 between tumor and acinar areas (m/z 380.1065, Fig. 2A) as well as additional metabolites M16 and M6 (Fig. 2B).

Relative erlotinib levels in tumors do not correlate with overall survival or differentiation status

Next, we investigated whether survival or tumor differentiation correlates with erlotinib peak intensities and distribution in PDAC. Therefore, we subjected 12 *Kras*^{G12D};*p53*^{KO} mice to weekly MRI exams starting at week 5 of age to determine tumor onset. Upon a defined tumor burden (200–400 mm^3), mice were treated with either only 100 mg/kg erlotinib daily ($n = 5$ mice) or with 50 mg/kg erlotinib daily plus four single doses of gemcitabine separated each by 3 days ($n = 7$). Mice were treated daily and received one additional single dose of erlotinib upon reaching no-go criteria 1 hour before sacrifice (schematic treatment overview Fig. 3A). Parameters obtained included survival time, overall erlotinib peak intensities in two independent randomly chosen pancreatic tumor sections that were at least 5 mm apart, and tumor grade as determined by a pancreatic pathologist (Table 1). Survival and histologic analysis of the tumor sections did not show significant differences between mono- or combination-treated tumor-bearing animals as previously reported (ref. 5; Supplementary Fig. S2A).

Overall, average erlotinib peak intensities between two sections from different regions of individual mice showed high correlation, indicating representative drug distribution in single sections (Supplementary Fig. S2B). However, overall intratumoral erlotinib peak intensities did not correlate with either overall survival or tumor grade (Fig. 3C and Supplementary Fig. S2C).

Localization of erlotinib-treated mice correlates with overall survival

We next examined drug distribution in PDAC of the 12 long-term–treated mice in more detail. Tumor areas with more atypical glands showed higher average peak intensities of erlotinib than areas with a higher stroma content. To test this hypothesis, we developed a tissue image analysis algorithm that classified morphologic features as "glandular," i.e., having a more differentiated epithelial morphology, or as "desmoplastic," i.e., with no obvious epithelial proportions and high stroma content, based on the density and relative distance of cell nuclei to each other (Fig. 3B). A second algorithm was implemented to quantify the percentage of tissue that showed the presence of the relative erlotinib peak intensity in the two-dimensional tissue distribution overlay image as exemplified in Fig. 3B (middle; overlay of histology and average peak intensity) and quantified as a binary function of being present in that morphologic area or not (Fig. 3B, right side). We next determined the percentage of erlotinib presence in glandular or desmoplastic areas of the tumors and correlated these with the duration of study treatment. Both, the overall percentage of glandular areas in the tumors and the percentage of drug found in these areas significantly correlated with the survival of the treated mice ($n = 12$, Fig. 3C), although the amount of glandular complexes in the tissue and the percentage of them containing drug did not correlate (Supplementary Fig. S2D). This indicates that the higher the percentage of atypical glands in PDAC tissue, the higher the amount of intratumoral drug and also the higher the survival in respective individual mice.

Discussion

In this study, we evaluated MALDI-based drug imaging for morphologic analysis of drug tissue distribution on a cellular level in a complex tumor using a well-established GEMM of aggressive PDAC with high desmoplasia. Underlying evidence for this approach stems from increasing evidence for the tumor microenvironment as a major factor in drug delivery determining outcome as previously described in PDAC with its abundant desmoplasia (3,8,9). However, other variables affecting drug metabolism and stabilization of the respective drug have been described (16); thus, the clinical translation remains challenging.

Because of its practical simplicity and ability to gain reliable information, even from the smallest tissue amounts, which may also originate from endoscopic biopsies from patients for MALDI drug imaging, the application of MALDI IMS to determine the tissue distribution of drugs could have a dramatic impact on both drug discovery and development and, as shown by our study, for therapy response prediction.

In this study, we focused on imaging of erlotinib, which is approved for targeted therapy in PDAC *albeit* with only moderate

Published OnlineFirst January 28, 2016; DOI: 10.1158/1535-7163.MCT-15-0165

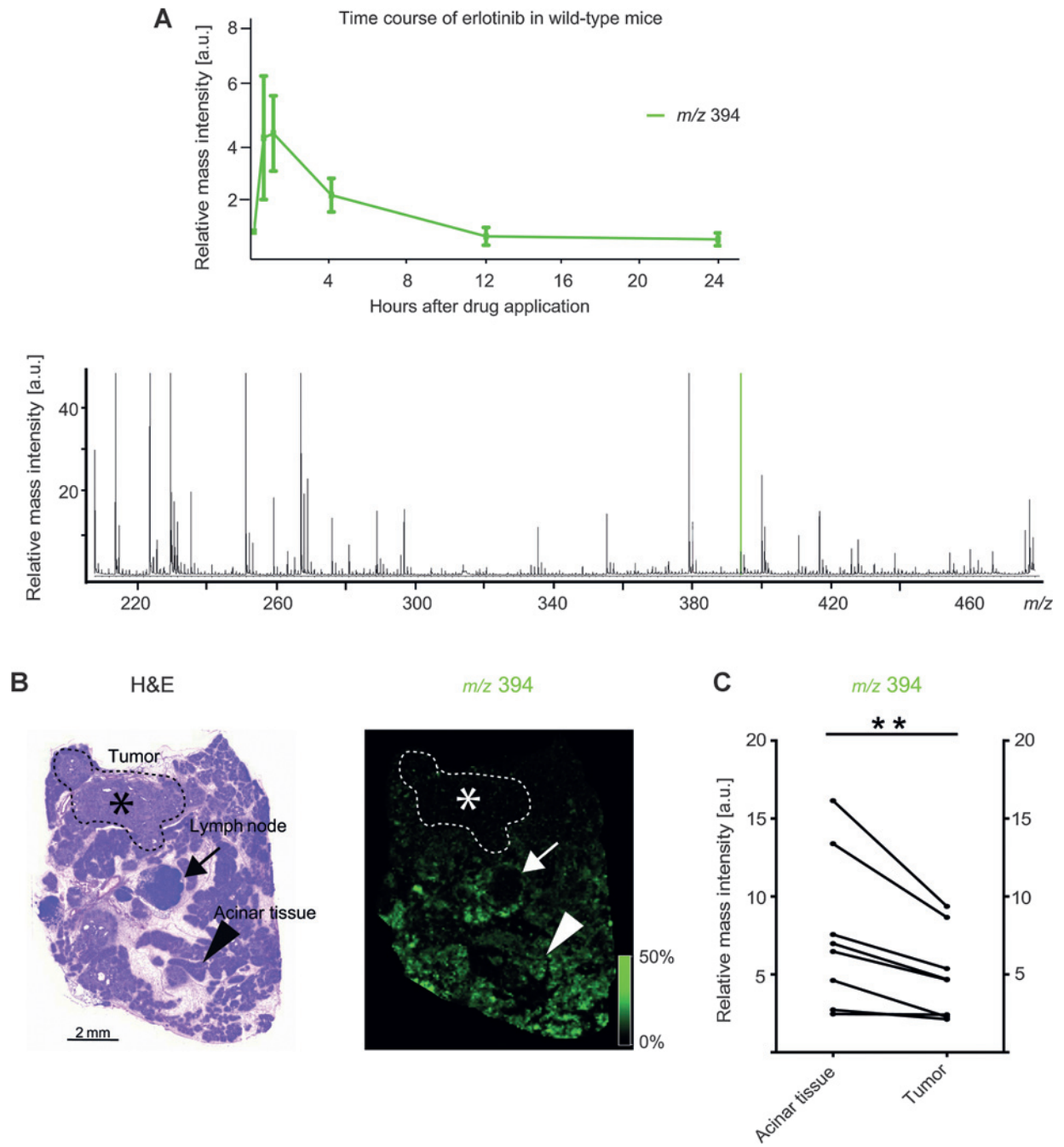

Figure 1.
A, time course of relative levels of erlotinib (*m/z* 394, green line) in murine WT pancreata at indicated time points after oral application. Untreated mice served as baseline, whereas mice treated with the vehicle methylcellulose only were measured at each time point to ensure specificity of the measured peaks. A total of 600 spectra per mouse were extracted and imported into ClinProTools to determine relative mass intensities for erlotinib; $n = 3$ mice per time point. B, representative average mass spectrum, histology, and corresponding revisualizations of erlotinib (*m/z* 394) in a pancreatic section of a 6-week-old $Kras^{G12D};p53^{KO}$ mouse containing an area with invasive PDAC, normal acinar tissue, and a lymph node. Scale bar, 2 mm. C, erlotinib (*m/z* 394) showed significantly ($P = 0.0078$) higher intensities in normal-appearing acinar areas than in tumor tissue. ROIs were defined for healthy acinar tissue and PDAC and 500 randomly chosen spectra per region extracted and processed with ClinProTools to obtain visual and statistical data about distribution of erlotinib.

effectiveness (17). Small-molecule inhibitors have been analyzed using this method including lapatinib and nevirapine in a mimetic tissue model with parallel dosed tissue sections to quantify drug amounts and to determine a tissue's effects on analyte extraction and ion suppression (18). Erlotinib has previously been studied using MALDI IMS,(19), *albeit* not in a long-term–treated complex disease model. Its distribution in healthy rat liver, spleen, and muscle resembled

Published OnlineFirst January 28, 2016; DOI: 10.1158/1535-7163.MCT-15-0165

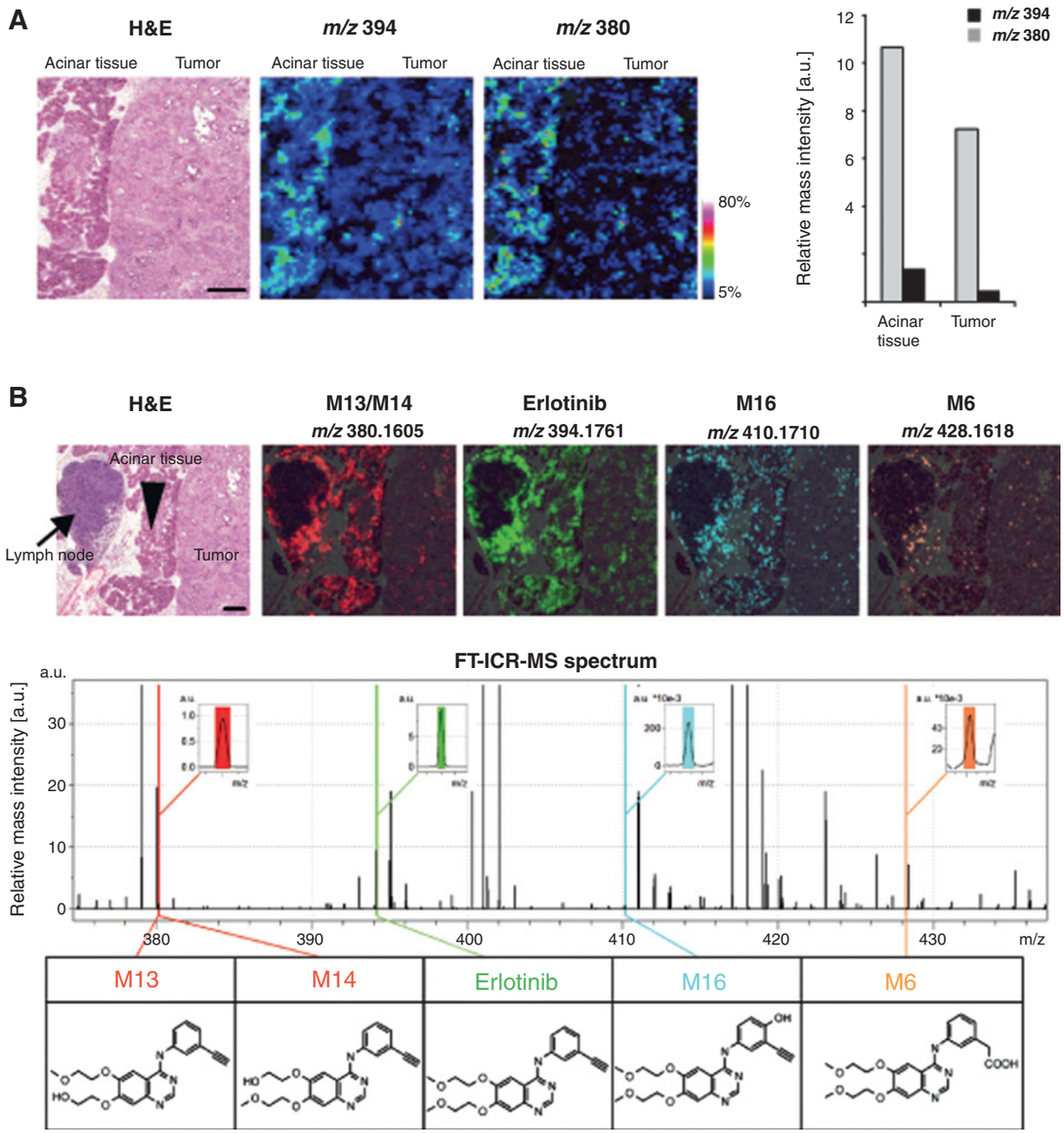

Figure 2.
A, relative quantification of erlotinib and the demethylative metabolites M13/M14. MALDI FT-ICR MSI detects erlotinib and related metabolites M13/M14 in acinar tissue and tumor in a 6-week-old *Kras*^{G12D};*p53*^{KO} mouse. With relative quantification, both erlotinib and the metabolites M13/M14 show higher intensity in acinar regions. Moreover, M13/M14 represent lower abundancy compared with the parent drug erlotinib. M14 is the pharmacologically active metabolite of erlotinib. Scale bar, 500 μm. B, MALDI FT-ICR imaging data and representative average MS spectrum of erlotinib and related metabolites, M13, M14, M16, and M6. H&E staining of a pancreatic section of a 6-week-old *Kras*^{G12D};*p53*^{KO} mouse shows invasive PDAC, normal acinar tissue, and a lymph node. Erlotinib is present at moderate levels in the tumor area, while we found higher levels of erlotinib in acinar region and the subcapsular sinus of lymph node. MALDI FT-ICR MSI enables simultaneous detection of low abundant metabolites peaks, M13, M14, M16, and M6, which represent similar distributions as the parent drug. Please note that M13 and M14 are isomers with identical molecular mass, which cannot be distinguished by current MALDI MSI analysis. Scale bar, 500 μm.

autoradiographic results. In 2011, differences in distribution of erlotinib in three different lung cancer tumor phenotypes were reported (20), and in 2013, drug distribution of erlotinib and other molecules in the microenvironmental tissue compartments of lung cancer that were either submerged or spotted with the compounds was investigated (21).

In our study, erlotinib was administered orally as used in clinical administration. This way, tissue delivery and distribution

Published OnlineFirst January 28, 2016; DOI: 10.1158/1535-7163.MCT-15-0165

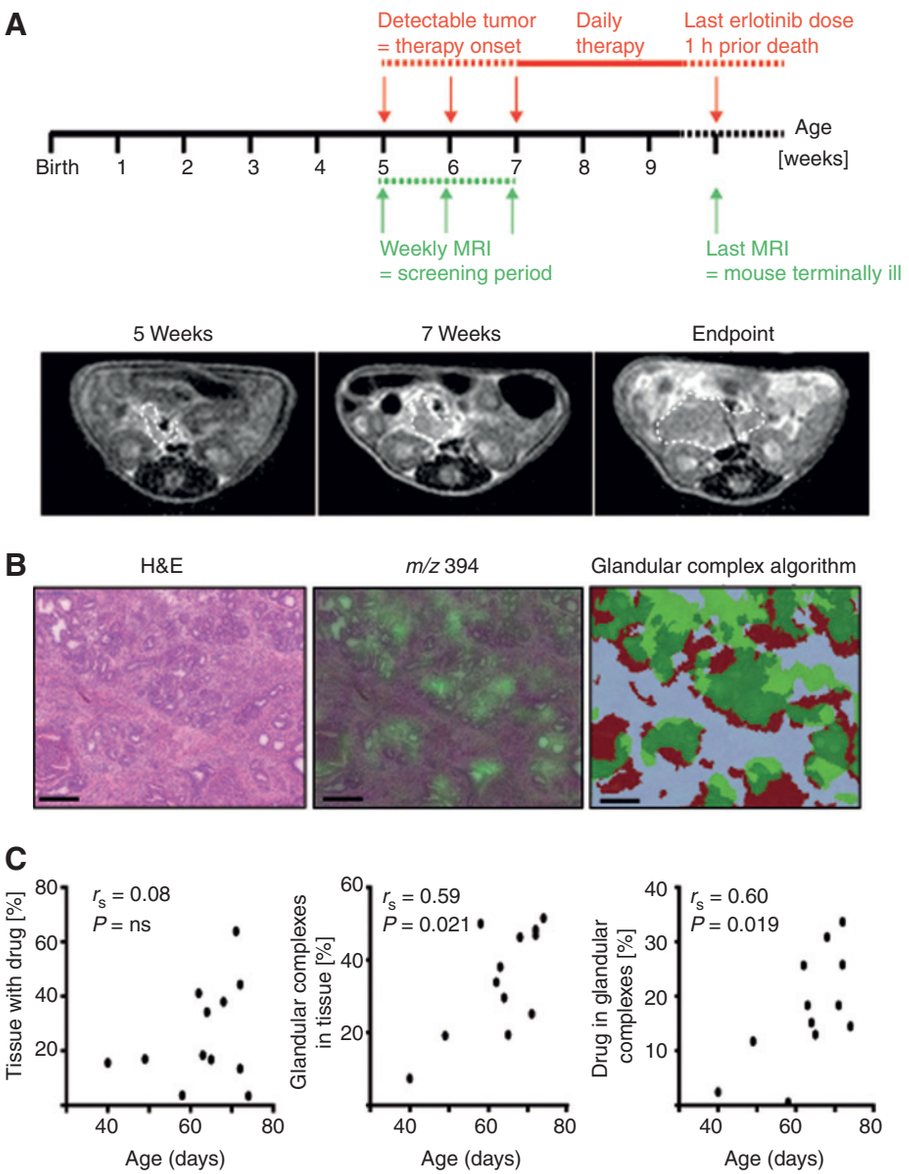

Figure 3.
A, schematic of treatment and measurements in long-term–treated $Kras^{G12D};p53^{KO}$ mice. Below, the representative MRI scan shows the pancreas at start of the measurement and during progression at indicated time points. White dotted line indicates pancreas/tumor area. B, representative image of pancreatic histology (left), erlotinib revisualization measured with MALDI imaging (green, middle picture), and tissue analysis cluster algorithm (right picture, light green indicating areas with detectable erlotinib mass, dark red indicating areas classified as "glandular," and dark green indicating areas with an overlap between those). Scale bars, 200 µm. C, correlation analysis of survival with overall drug levels in tissue (left, P = ns, $r_s = 0.08$) with percentage of atypical glands in tumor areas (middle, $P = 0.021$, $r_s = 0.59$) and percentage of drug (right, $P = 0.019$, $r_s = 0.60$). Each data point represents one analyzed section per mouse ($n = 12$ mice total).

of erlotinib are dependent on the metabolism of the drug *in vivo*, therefore allowing us to draw biologically meaningful conclusions about erlotinib distribution. We observed rapid tissue elimination of the parent drug already after 1 hour in WT mice. To correlate intratumoral erlotinib tissue distribution patterns with effectiveness of the drug in a preclinical trial setting—which has to our knowledge not been reported before—we thus decided to administer one more single dose of erlotinib to mice before sacrifice, assuming, although not proven, that distribution of this last erlotinib dose would more reliably reflect drug distribution in the tumors. Even though we cannot follow tissue distribution over time, which would be potentially possible by procuring biopsies over the treatment course, our study describes reliable spatial distribution of erlotinib in a clinically relevant setting.

The method described here enables multimodal analysis of intratumoral drug levels, including high spatial resolution and drug metabolism (22,23). Application of MALDI IMS for imaging of pharmaceutical-unlabeled compounds has been of great interest since introduction of the technology (24,25). The emerging technique of MALDI IMS has the capability to distinguish between parent drug and metabolites while maintaining spatial distribution in tissues. MALDI drug imaging is often considered as a targeted approach in MSI, because the method is designed to detect specific drugs of interest within a sample. Autoradiography is also used to examine *in situ* distribution either in whole animals (whole-body autoradiography) or on the cellular level (microautoradiography). As these methods need labeling of the drug in contrast with MALDI IMS, they are not very suitable for long-term treatment studies. Homogenization- and separation-based LC-MS of tissue samples effectively and accurately allow for the identification and quantification of drugs and their metabolites, but result in the loss of spatial information. Absolute quantification is highly desired for pharmacologic studies. However, quantification using MSI is still a challenging research area due

Table 1. Overview of mice in the preclinical therapy trial

Mouse number	Group	Responder according to MRI	Age in days	Relative intensity erlotinib region 1	Relative intensity erlotinib region 2	Tumor stage	Anaplastic or sarcomatoid	ADM	Necrosis
60884	M		49	2.167	1.8032	G2			
60894	M	x	65	3.7494	3.2366	G2	s	x	
60895	M		58	5.8275	5.4462	G2			x
60908	M		63	6.613	12.5681	G2	a	x	
60904	M		72	4.7134	3.9381	G2	a + s	x	
60911	C		72	10.3315	4.2725	G2 + G3			
60950	C		64	4.3307	5.1656	G1 + G2 + G3			x
60965	C		71	3.3149	5.2965	G2		x	x
61018	C	x	74	2.3313	3.0282	G2			
61029	C	x	62	2.9096	3.1248	G2		x	
61025	C		40	3.7528	2.5548	G2 + G3		x	
61021	C	x	68	6.2353	4.2742	G2			

NOTE: Depicted are assigned mouse number, treatment group, MRI response, age in days, relative overall erlotinib levels in two independent regions, and tumor grading according to expert pancreatic pathologists (I. Esposito and K. Steiger). KrasG12D;p53KO mice were treated as indicated in Fig. 3A.
Abbreviations: a, anaplastic; s, sarcomatoid; ADM, acino-ductal metaplasia; C, combination therapy erlotinib and gemcitabine; G1, G2, G3, tumor staging according to pathologist; M, monotherapy erlotinib only; x, happened event.

to the limitations of MSI technology, such as substance-specific extraction and ionization, tissue-specific ion suppression, and matrix-specific deposition and properties. We have instead used relative quantification, which sufficiently revealed the potential impact of erlotinib levels in glandular structures on the survival of mice.

MALDI-TOF (Ultraflex) has limited mass resolution and accuracy, and only the parent drug can be detected using the Ultraflex. However, information regarding related metabolites is also highly informative and an increasingly recognized influencing factor. To ensure specificity, we performed additional high mass resolution MALDI FT-ICR analysis. In addition, a previous study by Huber and colleagues (26) has proven the high sensitivity and specificity of the applied method to detect erlotinib in tissue.

In our study, we find considerably less erlotinib in PDAC compared with healthy pancreatic tissue. Relative erlotinib peak intensities within the tumors vary highly, suggesting additional factors that influence drug distribution and intensity. Although overall tumor grading did not differ between the mice, we found that mice harboring PDAC with increased numbers of atypical glands and higher intraglandular erlotinib peak intensities showed an increased survival. Whether this is due to less aggressive tumors, tumors with less stroma, and potentially lower interstitial pressure, differences in drug response or indeed the measured increased drug presence remain to be determined.

There are further limitations to be considered. Survival in this aggressive GEMM is short, and effects on survival are difficult to address. Second, we did not acquire suitable biopsy tissue early after therapy start, as one would envision in a clinical trial and needed for evaluation of intratumoral erlotinib as a predictive biomarker. This study shows that drug distribution as well as metabolism in tumors is highly complex and needs to be investigated in great detail on a cellular level, for which we find MALDI IMS a highly suitable method. Investigating the influence of the desmoplastic reaction in low versus high desmoplastic tumors or the effect of stroma-modulating drugs on drug distribution and therapy response are clinically highly anticipated study aims that could potentially be approached using this method.

In conclusion, MALDI drug imaging provides an excellent approach to study drug delivery, spatial distribution, and drug metabolism in great detail in complex preclinical models and in future clinical trials.

Disclosure of Potential Conflicts of Interest

No potential conflicts of interest were disclosed.

Authors' Contributions

Conception and design: B.M. Grüner, I. Winkelmann, R. Braren, R.M. Schmid, A. Walch, J.T. Siveke

Development of methodology: B.M. Grüner, I. Winkelmann, A. Feuchtinger, I. Esposito, A. Walch

Acquisition of data (provided animals, acquired and managed patients, provided facilities, etc.): B.M. Grüner, I. Winkelmann, A. Feuchtinger, A. Herner, E. Kalideris, M. Aichler, I. Esposito, J.T. Siveke

Analysis and interpretation of data (e.g., statistical analysis, biostatistics, computational analysis): B.M. Grüner, I. Winkelmann, A. Feuchtinger, N. Sun, B. Balluff, K. Steiger, M. Aichler, I. Esposito, A. Walch, J.T. Siveke

Writing, review, and/or revision of the manuscript: B.M. Grüner, I. Winkelmann, A. Feuchtinger, N. Sun, B. Balluff, R. Braren, M. Aichler, I. Esposito, A. Walch

Administrative, technical, or material support (i.e., reporting or organizing data, constructing databases): N. Teichmann, E. Kalideris

Study supervision: R. Braren, R.M. Schmid, A. Walch, J.T. Siveke

Acknowledgments

The authors thank Pawel K. Mazur for insightful comments and fruitful discussions and Claudia-Mareike Pflueger and Mathilde Neuhofer for excellent technical assistance. Parts of the results of this study are publicly available in the PhD thesis of B.M. Grüner at the university library of the Technical University Munich.

Grant Support

This work was supported by the collaborative research center SFB 824, German Research Foundation (DFG) "Imaging for Selection, Monitoring and Individualization of Cancer Therapies" (project C4 to J.T. Siveke and Z2 to A. Walch), German Research Foundation grant # HO 1254/37 (to A. Walch), German Cancer Aid (Deutsche Krebshilfe #109992 to J.T. Siveke), the German Federal Ministry of Education and Research [National Genomic Research Network (NGFN-Plus), 01GS08115 to J.T. Siveke and R.M. Schmid], the German Cancer Consortium (DKTK; to R.M. Schmid and J.T. Siveke), and the European Community's Seventh Framework Programme (FP7/CAM-PaC) under grant agreement # 602783 to J.T. Siveke. B.M. Grüner was supported by the 2014 Pancreatic Cancer Action Network–AACR Fellowship in memory of Samuel Stroum #14-40-25-GRUE.

The costs of publication of this article were defrayed in part by the payment of page charges. This article must therefore be hereby marked *advertisement* in accordance with 18 U.S.C. Section 1734 solely to indicate this fact.

Received February 23, 2015; revised November 13, 2015; accepted December 6, 2015; published OnlineFirst January 28, 2016.

Published OnlineFirst January 28, 2016; DOI: 10.1158/1535-7163.MCT-15-0165

References

1. Hidalgo M. Pancreatic cancer. N Engl J Med 2010;362:1605–17.
2. Mazur PK, Siveke JT. Genetically engineered mouse models of pancreatic cancer: unravelling tumour biology and progressing translational oncology. Gut 2012;61:1488–500.
3. Olive KP, Jacobetz MA, Davidson CJ, Gopinathan A, McIntyre D, Honess D, et al. Inhibition of Hedgehog signaling enhances delivery of chemotherapy in a mouse model of pancreatic cancer. Science 2009;324:1457–61.
4. Balluff B, Rauser S, Ebert MP, Siveke JT, Hofler H, Walch A. Direct molecular tissue analysis by MALDI imaging mass spectrometry in the field of gastrointestinal disease. Gastroenterology 2012;143:544–9.
5. Ardito CM, Gruner BM, Takeuchi KK, Lubeseder-Martellato C, Teichmann N, Mazur PK, et al. EGF receptor is required for KRAS-induced pancreatic tumorigenesis. Cancer Cell 2012;22:304–17.
6. Faller BA, Burtness B. Treatment of pancreatic cancer with epidermal growth factor receptor-targeted therapy. Biologics 2009;3:419–28.
7. Zahorowska B, Crowe PJ, Yang JL. Combined therapies for cancer: a review of EGFR-targeted monotherapy and combination treatment with other drugs. J Cancer Res Clin Oncol 2009;135:1137–48.
8. Minchinton AI, Tannock IF. Drug penetration in solid tumours. Nat Rev Cancer 2006;6:583–92.
9. Tredan O, Galmarini CM, Patel K, Tannock IF. Drug resistance and the solid tumor microenvironment. J Natl Cancer Inst 2007;99:1441–54.
10. Nakhai H, Sel S, Favor J, Mendoza-Torres L, Paulsen F, Duncker GI, et al. Ptf1a is essential for the differentiation of GABAergic and glycinergic amacrine cells and horizontal cells in the mouse retina. Development 2007;134:1151–60.
11. Hingorani SR, Wang L, Multani AS, Combs C, Deramaudt TB, Hruban RH, et al. Trp53R172H and KrasG12D cooperate to promote chromosomal instability and widely metastatic pancreatic ductal adenocarcinoma in mice. Cancer Cell 2005;7:469–83.
12. Marino S, Vooijs M, van Der Gulden H, Jonkers J, Berns A. Induction of medulloblastomas in p53-null mutant mice by somatic inactivation of Rb in the external granular layer cells of the cerebellum. Genes Dev 2000;14:994–1004.
13. Ling J, Johnson KA, Miao Z, Rakhit A, Pantze MP, Hamilton M, et al. Metabolism and excretion of erlotinib, a small molecule inhibitor of epidermal growth factor receptor tyrosine kinase, in healthy male volunteers. Drug Metab Dispos 2006;34:420–6.
14. Bardeesy N, Aguirre AJ, Chu GC, Cheng KH, Lopez LV, Hezel AF, et al. Both p16(Ink4a) and the p19(Arf)-p53 pathway constrain progression of pancreatic adenocarcinoma in the mouse. Proc Natl Acad Sci U S A 2006;103:5947–52.
15. Bardeesy N, DePinho RA. Pancreatic cancer biology and genetics. Nat Rev Cancer 2002;2:897–909.
16. Frese KK, Neesse A, Cook N, Bapiro TE, Lolkema MP, Jodrell DI, et al. nab-Paclitaxel potentiates gemcitabine activity by reducing cytidine deaminase levels in a mouse model of pancreatic cancer. Cancer discovery 2012;2:260–9.
17. Moore MJ, Goldstein D, Hamm J, Figer A, Hecht JR, Gallinger S, et al. Erlotinib plus gemcitabine compared with gemcitabine alone in patients with advanced pancreatic cancer: a phase III trial of the National Cancer Institute of Canada Clinical Trials Group. J Clin Oncol 2007;25:1960–6.
18. Groseclose MR, Castellino S. A mimetic tissue model for the quantification of drug distributions by MALDI imaging mass spectrometry. Anal Chem 2013;85:10099–106.
19. Signor L, Varesio E, Staack RF, Starke V, Richter WF, Hopfgartner G. Analysis of erlotinib and its metabolites in rat tissue sections by MALDI quadrupole time-of-flight mass spectrometry. J Mass Spectrom 2007;42:900–9.
20. Marko-Varga G, Fehniger TE, Rezeli M, Dome B, Laurell T, Vegvari A. Drug localization in different lung cancer phenotypes by MALDI mass spectrometry imaging. J Proteomics 2011;74:982–92.
21. Vegvari A, Fehniger TE, Rezeli M, Laurell T, Dome B, Jansson B, et al. Experimental models to study drug distributions in tissue using MALDI mass spectrometry imaging. J Proteome Res 2013;12:5626–33.
22. Khatib-Shahidi S, Andersson M, Herman JL, Gillespie TA, Caprioli RM. Direct molecular analysis of whole-body animal tissue sections by imaging MALDI mass spectrometry. Anal Chem 2006;78:6448–56.
23. Stoeckli M, Staab D, Schweitzer A, Gardiner J, Seebach D. Imaging of a beta-peptide distribution in whole-body mice sections by MALDI mass spectrometry. J Am Soc Mass Spectrom 2007;18:1921–4.
24. Castellino S, Groseclose MR, Wagner D. MALDI imaging mass spectrometry: bridging biology and chemistry in drug development. Bioanalysis 2011;3:2427–41.
25. Norris JL, Caprioli RM. Analysis of tissue specimens by matrix-assisted laser desorption/ionization imaging mass spectrometry in biological and clinical research. Chemical reviews 2013;113:2309–42.
26. Huber K, Aichler M, Sun N, Buck A, Li Z, Fernandez IE, et al. A rapid ex vivo tissue model for optimising drug detection and ionisation in MALDI imaging studies. Histochem Cell Biol 2014;142:361–71.

Published OnlineFirst January 28, 2016; DOI: 10.1158/1535-7163.MCT-15-0165

Molecular Cancer Therapeutics

Modeling Therapy Response and Spatial Tissue Distribution of Erlotinib in Pancreatic Cancer

Barbara M. Grüner, Isabel Winkelmann, Annette Feuchtinger, et al.

Mol Cancer Ther 2016;15:1145-1152. Published OnlineFirst January 28, 2016.